Raman Imaging in Cell Membranes, Lipid-rich Organelles and Lipid Bilayers

Aleem Syed and Emily A. Smith

Department of Chemistry, Iowa State University and The Ames Laboratory, U.S. Department of Energy, Ames, Iowa 50011-3111, United States

email:esmith1@iastate.edu

Keywords

Coherent anti-Stokes Raman scattering; stimulated Raman scattering; surface-enhanced Raman scattering; tip-enhanced Raman scattering; alkyne-tags; deuterium labeling

Abstract

Raman-based optical imaging is a promising analysis tool for non-invasive, label-free chemical imaging of lipid bilayers and cellular membranes. Imaging using spontaneous Raman scattering suffers from a low intensity that hinders its use in some cellular applications. However, developments in coherent Raman imaging, surface-enhanced Raman imaging, and tip-enhanced Raman imaging have enabled video rate imaging, excellent detection limits, and nanometer spatial resolution, respectively. After a brief introduction to these commonly used Raman imaging techniques for cell membrane studies, selected applications of these modalities for chemical

imaging of membrane proteins and lipids are reviewed. Finally, recent developments in chemical tags for Raman imaging and their applications in the analysis of selected cell membrane components are summarized. On-going developments towards improving the temporal and spatial resolution of Raman imaging and small-molecule tags with strong Raman scattering cross-sections continue to expand the utility of Raman imaging for diverse cell membrane studies.

1. INTRODUCTION

The cell membrane is a complex organelle that contains various proteins, lipids, and small molecules with unique chemical signatures. In the model proposed by Singer and Nicholson in 1972, the cell membrane is assumed to be a two-dimensional uniform fluid where membrane proteins diffuse freely in a sea of lipid [1]. However, the scientific understanding of the cell membrane has evolved over time. In 2014, Nicholson updated his original membrane model by adding important lipid and protein interactions that are essential for cellular functions [8].

A simplified schematic of the cell membrane is shown in Figure 1. Cell membrane properties, such as the lipid distribution and membrane protein concentration, have been used as a biomarker for pathological conditions [9, 10]. Although there are imaging techniques that can provide atomic resolution, including a variety of scanning probe microscopies, optical techniques remain leading imaging methods for characterizing biological samples, and in particular are suited to measure the dynamics of biological systems. The ease of implementation, minimal invasiveness and possibility for high selectivity make optical techniques such as fluorescence and Raman imaging unparalleled for measuring cell membrane compositions, structures and dynamics.

The Raman effect was first identified by Raman and Krishnan where they reported, "…in every case in which light is scattered by the molecules in dust-free liquids or gasses, the diffuse radiation of the ordinary kind, having the same wavelength as the incident beam, is accompanied by a modified scattered radiation of degraded frequency" [11]. As shown in Figure 2a, upon interaction with a photon, a molecule generates scattered light with no change in the wavelength (called Rayleigh scattering, ω_r) or with an altered wavelength (called Raman scattering). If the altered wavelength is longer than the incident light, it is called Stokes scattering (ω_s) otherwise it

is called anti-Stokes scattering (ω_{as}). The change in the wavelength encodes the identity of the functional groups within the molecule.

In terms of current and historical usage, fluorescence imaging is considered a gold standard for optical imaging studies of the cell membrane. Despite this, there are advantages of Raman over fluorescence imaging in the context of cell membrane studies. (1) Raman imaging can be performed in a label-free format, and, if a label is used, the label can be as small as two atoms, which may minimize the disruption of biological function. (2) Raman imaging does not suffer from photobleaching as is common in fluorescence imaging. (3) Raman peaks are narrow (*e.g.*, a few nanometers) compared to fluorescence peaks (*e.g.*, 50-100 nm) enabling a higher degree of multiplexing, and in addition (4) a single laser enables simplified Raman instrumentation for multiplexing.

Almost 90% of the Raman peaks from the spectrum of a human cell are in the fingerprint spectral region between 500 cm^{-1} to 1800 cm^{-1} (Figure 2b) [12]. The remaining peaks are in the spectral window 2700 cm^{-1} to 3100 cm^{-1}. The majority of the peaks are assigned to lipids, proteins, and nucleic acids. Using Raman imaging multiple cellular components can be imaged simultaneously without a label. The spectral region between 1800 cm^{-1} to 2700 cm^{-1} is termed the cell-silent region, where no appreciable cellular peaks are located.

The spontaneous Raman signal is generally considered to be weak (1 photon in every 10^6 to 10^8 scattered photons), which has limited imaging speeds and utility for measuring the fast dynamics of the cell membrane. Various approaches have been developed over the years to increase the imaging speed, which were recently reviewed [13]. Herein, the recent developments in the application of Raman imaging for cell membrane studies are reviewed. After a brief

introduction to the basic principles of the commonly used Raman modalities for cell membrane studies, selected applications of these methods to cell membrane applications are reviewed. The Raman imaging approaches reviewed here in the context of cell membrane studies are: (1) coherent Raman scattering, (2) surface-enhanced Raman scattering and (3) tip-enhanced Raman scattering. Instrumentation for Raman imaging is not discussed here, and the reader is directed to appropriate reviews on the topic [14-16].

A second concern with Raman imaging is that label-free imaging, while sometimes advantageous, can also make it difficult to measure a single membrane component among all the components in the cell membrane. This has been addressed by introducing new classes of Raman tags that are reviewed in the final section of this review. Finally, the current areas of development in Raman imaging that make this imaging modality an even more attractive option for cell membrane studies are summarized.

2. COMMON RAMAN-BASED IMAGING METHODS FOR CELL MEMBRANE STUDIES

2.1. Coherent Raman Scattering

In this section, imaging techniques based on coherent Raman scattering (CRS) are discussed as an alternative to the relatively weak spontaneous Raman signal. The two most common imaging formats under the CRS family are coherent anti-Stokes Raman scattering (CARS) and stimulated Raman scattering (SRS).

In most CARS experiments three excitation fields denoted as the pump at ω_p, Stokes at ω_s and probe at ω_{pr} are used (Figure 2a). The frequency difference between the pump and Stokes fields (ω_p - ω_s) corresponds to a specific vibrational mode in the sample and a CARS signal is generated at $\omega_{pr}+(\omega_p-\omega_s)$. In most experiments, both the pump and probe fields are generated from the same source and are the same frequency. CARS was first reported in 1965, and the first CARS microscope was demonstrated in 1982 [17, 18]. CARS research underwent a renaissance in 1999 when Xie and coworkers reported 3D CARS with collinear femtosecond laser excitation [19]. Various imaging modalities have been reported for CARS such as narrowband, broadband and multiplex CARS, to list few. CARS imaging at video rate has been reported for lipid contrast [20].

The spontaneous Raman signal is isotropic, however, the majority of the CARS signal is forward directed (*i.e.*, the signal is directional). This facilitates a high detection efficiency in the transmissive direction. Since the detected signal is at a lower wavelength, the CARS signal does not compete with the fluorescence background, which can otherwise be problematic for biological samples. However, CARS suffers from an inherent non-resonant background that makes it difficult to retrieve the signal. Various approaches have been developed to tackle the non-resonant background in CARS. When the signal of interest emanates from features that are smaller than the wavelength of light, non-resonant background from the bulk is suppressed by using the signal collected in the epi-direction rather than detecting forward CARS, although non-resonant background from sub-wavelength features is not eliminated [21]. Frequency modulation CARS has been successfully implemented to image the distribution of deuterium-labeled oleic acid in human lung cancer cells with significantly lower non-resonant background compared to typical CARS [22]. The theoretical framework and instrument developments to address issues such as non-resonant background have been reviewed previously [22-26].

Although the imaging speed is significantly improved for CRS-based Raman imaging over spontaneous Raman imaging, the limit of detection is problematic for some applications. Lipids have been the primary focus of CRS-based imaging [19, 27-31]. In 2002, Xie and coworkers used CARS to study the changes in the cell membrane during apoptosis in NIH 3T3 cells using the aliphatic C-H vibration [32]. They recorded forward-detected CARS and epi-detected CARS simultaneously to obtain high contrast images of features that are larger and smaller than the excitation wavelength, respectively. Similarly, Kano has imaged various organelles including the cell membrane in HeLa cells with CARS using the C-H vibrational mode [33]. CARS has also been used to image the myelin sheath of neural cells. The myelin sheath is a multilamellar membrane around the axons. The degradation of myelin is linked to neurodegenerative diseases such as multiple sclerosis. Due to the abundant quantities of lipids, myelin can be imaged *in vivo* using CARS without exogenous labels [34-36].

CARS has been coupled with other nonlinear techniques for multimodal imaging. In combination with two-photon excitation fluorescence and sum-frequency generation (SFG), Cheng and coworkers used CARS to image the signal from the CH_2-rich membranes of endothelial and smooth muscle cells to visualize the arterial wall [37]. Similarly, Prasad and coworkers studied the organization of macromolecules such as protein, lipids, DNA and RNA in HeLa cells [38]. They used CARS to image the distribution of proteins and lipids and two-photon fluorescence to image labeled DNA and RNA.

As a demonstration of dynamic imaging, Xie and coworkers studied the structural changes in lipid droplets in live cells over several hours using CARS [39]. They reported that the observed contrast in CARS is as good as fluorescence microscopy with Oil Red O staining. In a follow-up study, they measured the dynamics of lipid droplets using CARS in real-time [40]. They observed

both sub-diffusion and active transport of lipid droplets along microtubules. The effect of interactions with mitochondria on the dynamics of lipid droplets has been studied with CARS. [39, 40]. Similarly, Pezacki and coworkers studied the interaction between hepatitis C virus core protein and lipid droplets. This interaction is one of the pathways that viruses use to proliferate with components from the host cells [41]. Zumbush and coworkers studied the diffusion of lipid droplets in live HeLa cells at video-rate for several hours [31].

The lipid organization in the cell membrane is not uniform; heterogeneous lipid domains exist in the cell membrane. These domains enable specific proteins to form clusters in the cell membrane, which may be critical for their function [42, 43]. Measuring the lipid compositions of these domains will advance our knowledge of cell membrane organization. To this end, lipid domain compositions have been analyzed by several groups using CARS in artificial lipid environments. Müller and coworkers used multiplex CARS to acquire spectra from lipid monolayers and bilayers [44]. They were able to measure lipids selectively from either leaflet of an asymmetric bilayer. Using giant unilamellar vesicles as the model cell membrane, Potma and Xie demonstrated lipid domain imaging with CARS [45]. Cheng and coworkers imaged deuterated acyl chains with epi-CARS to analyze various lipid domains in supported bilayers [46]. They have also modulated cholesterol content to study the effect of cholesterol on the lipid organization in supported bilayers. Also, label-free CARS imaging was used for probing solid, liquid-ordered and liquid disordered domains by Cheng and coworkers [47]. The proof of concept studies in artificial lipid bilayers, described here, show the potential of CARS to unravel the lipid organization in the cell membrane.

Stimulated Raman spectroscopy (SRS) is another coherent Raman imaging technique. The increasing popularity of SRS is due in part to a simple interpretation of Raman data as the spectral

profile in SRS is similar to that of spontaneous Raman spectroscopy without non-resonant background. In an SRS experiment, two excitation fields designated as a pump at frequency ω_p and Stokes at frequency ω_s are used. As shown in Figure 2a, when the frequency difference between the pump and probe fields (ω_p - ω_s) matches a specific Raman-active molecular vibration in the sample, two changes occur. Stimulated Raman loss (SRL) is an intensity loss in the pump field at ω_p and stimulated Raman gain (SRG) is an intensity gain in the Stokes field at ω_s. The change in the intensities is measured as a signal in SRS through phase sensitive detection schemes. The SRS imaging speed is increased by the signal amplification that results when there is a local oscillator at the detection frequency. In 2010, Xie and coworkers reported video-rate SRS by improving the collection geometry for backscattered light that made it possible to image lipids and proteins at a speed of 25 frames/s [27]. For single frequency SRS imaging, the image acquisition speed can be 100-times faster than spontaneous Raman imaging using a line-shaped excitation profile and 10,000-times faster than spontaneous Raman imaging using a point-shaped excitation profile [48]. Although there is no non-resonant background present in SRS, factors such as noise, background from non-Raman processes, and photodamage affect the quality of the image. Various elegant approaches have been implemented to minimize these effects and have been reviewed by Cheng and coworkers [48]. Unlike CARS, the SRS signal is linearly dependent on concentration; quantitative information and concentration maps of multiple species can be obtained from hyperspectral/multiplex SRS data. In general, based on the prior knowledge of the sample, various chemometrics methods such as least-square fitting, principal component analysis and multivariate analysis have been used for quantitative analysis [49-51].

Similar to CARS, SRS has been used to image lipid and protein distributions in live cells. For example, as shown in Figure 3, Zhang *et al.* imaged lipids at 2845 cm^{-1} (Figure 3b) and proteins

at 1655 cm^{-1} (Figure 3c) in *Drosophila* cells and mammalian HEK293 and MCF-7 cell lines without any external labels [52]. Also, the authors were able to measure the peaks corresponding to nucleic acids at 785 cm^{-1} (Figure 3d) that are difficult to resolve with CARS due to the non-resonant background. Cheng and coworkers have coupled SRS to spontaneous Raman scattering [53, 54]. This combination provided the ability to obtain high-speed Raman images as well as detailed spectra at pixels of interest. In another study by the same research group, femtosecond pulse SRS was used to study lipid synthesis in CHO cells [55]. For this purpose, they used deuterated palmitic acid as a precursor for lipid synthesis, and newly formed lipid droplets were imaged through deuterated lipid mapping with SRS.

Liao *et al.* have successfully performed a compositional analysis of lipid droplets in live cancer cells using multiplex SRS, demonstrating the ability of SRS to image dynamic cellular components [56]. Lipid droplets are mainly constituted of cholesterol ester and triglycerides. In this study, the authors were able to estimate the percentage of cholesterol ester in stationary and moving lipid droplets. Further they have used multiplex SRS to study the dynamic conversion of retinol into retinoic acid in cancer cells. In retinoid metabolism, retinol is initially oxidized to retinaldehyde and then further oxidized to retinoic acid. The Raman peaks corresponding to retinol and retinoic acids appear at 1580 cm^{-1} and 1605 cm^{-1}, respectively, and they are distinct from the lipid peak at 1650 cm^{-1}. Thus, the authors could monitor the metabolic conversion of retinol by measuring Raman peaks at these three wavenumbers with multiplex SRS. In another study, Cheng and coworkers studied lipogenesis using deuterated glucose in pancreatic cancer cells [57]. Glucose in mammalian cells is used as an important energy source and a precursor for lipid synthesis. Isotopically labeled glucose can be used to study lipogenesis in live cells. Another dynamic event that has been investigated in live cells with SRS is choline metabolism. Choline is

involved in cell membrane formation, lipid transport and signaling. Min and coworkers imaged the choline metabolism in different types of cancer (Figure 4a-d) and embryonic (Figure 4e-h) cells using isotope labeled choline (choline-D_9) and SRS [59]. Similar to deuterium labeling, alkyne-tags are also incorporated in small metabolites. For example, the alkyne-tag phenyl-diyne was covalently attached to cholesterol to map the distribution of cholesterol in a live cell [60]. The phenyl-diyne tag is biologically inactive and generates strong Raman signal that enables detection of small metabolites from the complicated cellular background.

As nonlinear processes, CARS and SRS provide excellent 3D sectioning of the sample as the signal mainly originates from the center of the focal plane. However, the spatial resolution is still limited by the optical diffraction limit. Through super-resolution CARS imaging, a spatial resolution of 130 nm was achieved in the case of nanomaterials [61]. Inspired by stimulated emission depletion fluorescence microscopy, a ground state depletion approach has been implemented to achieve sub-diffraction spatial resolution in SRS for non-biological materials [62, 63]. These new methodologies have the potential to be applied to biological samples, and may be applied to study numerous membrane phenomena. The current detection limit for CRS-based imaging is still above 1 mM [26]. This sensitivity currently limits the application of CRS techniques to highly abundant species, such as lipids and some proteins in the cell membrane. Although new approaches are being developed to improve the spatial resolution of CRS methods, limited sensitivity may hinder our ability to probe small volumes and/or species of low abundance.

Given the complexity of the CRS instrumentation, applications in this field are generally limited to specialized labs. These techniques are unlikely to replace the most common optical imaging methods, although these techniques offer tremendous potential in biological imaging. For example, the ability to track cell membrane components with high spatial and temporal resolution

in a label-free format will enable the analysis of cell signaling pathways that are not feasible with current fluorescence-based approaches.

2.2. Surface-enhanced Raman Spectroscopy for Cell Membrane Studies

In this section of the review, we cover applications of surface-enhanced Raman spectroscopy (SERS) for imaging cell membrane proteins and lipids. In SERS, the signal from a Raman-active molecule is enhanced due to its vicinity (roughly a few nanometers) to a roughened or nanopatterned metal surface. Many metals have been reported to exhibit a SERS effect such as silver, gold, copper, and lithium [64-70]. The enhanced signal is commonly about a million times higher compared to the spontaneous Raman signal from the same molecule in solution. The enhancement factor is a combinatorial effect of electromagnetic and chemical enhancement mechanisms, with the former being the major contributor towards the overall enhancement [71, 72]. (For a historical perspective of SERS, please see the autobiography article by Richard Van Duyne in this volume).

SERS has been used to detect various analytes such as DNA bases, explosives, therapeutic agents, drugs, cells, spores and food additives. (For a perspective of the bioanalytical application of SERS, please see the review in this volume by Graham *et al.*). SERS detection limits can parallel those of fluorescence [73, 74], and SERS applications have appeared in domains that have been traditionally dominated by fluorescence detection. For example, Doorn and coworkers reported a flow cytometer that is capable of measuring SERS with integration times in the range of 10 μs to 20 μs [75].

Several groups have reported the label-free detection of purified proteins using SERS [76, 77]. The detection of a specific protein among a mixture requires a SERS probe functionalized with ligand or antibody for the target. An appropriately designed SERS probe will thus only bind to the target protein. The signal that is often recorded is from a Raman reporter, a molecule with a strong Raman signal that is commonly encapsulated within a polymer or silica coating onto the nanoparticle(s). The use of a Raman reporter with a resonant electronic transition coincident to the excitation wavelength further increases the signal. This effect is termed surface-enhanced resonance Raman spectroscopy (SERRS). SERS (or SERRS) is a heterogeneous phenomenon due to the random distribution of the regions on the nanoparticle(s) that produces the large enhancement, called hotspots. Thus, careful design of the SERS probe is necessary for a reproducible signal. The following discussion is focused on strategies to generate well-defined SERS probes for imaging components on the cell membrane.

There are many reported strategies to cluster metal nanoparticles to form well-defined hotspots. For example, DNA hybridization is used to form dimeric gold nanoparticles with tunable interparticle distances by varying the length of the DNA [78, 79]. In a study by Bazan and coworkers, dimeric spherical silver nanoparticles formed using an organic linker biphenyl-4,4-dithiol (DBDT) resulted in an overall 40% yield [80]. The aggregates were functionalized with aptamers that can be designed for the selective detection of biomolecules. Similarly, Fabris and coworkers formed dimeric gold nanoparticles using the dithiol DBDT, and the formation of higher order aggregates was inhibited by using a monothiol linker [81]. The resulting dimer was coated with polyethylene glycol (PEG) and further functionalized with arginine-glycine-aspartic acid tripeptide (*i.e.*, RGD) to specifically label αvβ3 integrins on the glioblastoma cell surface.

Another strategy to control the formation of hotspots in nanoparticle aggregates and to produce a more stable SERS signal is to use graphene oxide (GO) as a coating. Several features of GO make it an ideal candidate for forming well-defined metal clusters, including excellent water dispersion and superior molecular adsorption [82]. Silver nanoparticle/GO and gold nanoparticle/GO SERS probes have been used for cellular imaging [83-85]. Yang and coworkers reported folic acid-conjugated silver nanoparticle/GO SERS probes for imaging folate receptor (FR) on FR-positive HeLa cells [83]. GO has a relatively small Raman cross-section, so the use of GO in combination with a Raman reporter is beneficial. Chen and coworkers adsorbed the Raman reporter tris(2,2'-bipyridyl)ruthenium (II) chloride (RuBPy) on GO sheets [86]. Then, gold nanoparticles were formed on the GO surface, and the number of gold nanoparticles in the resulting SERS probe varied depending on the starting size of GO sheets. Since the thickness of the GO coating is about 1 nm, there is no significant loss of SERS signal from the RuBPy, and GO can readily be biofunctionalized for cellular imaging. For example, the ligand glutaraldehyde (GA) was adsorbed on the GO surface for Raman imaging of bacteria. The authors showed that an optimum metal nanoparticle cluster size enables the near-IR absorption of the SERS probe for the thermal ablation of bound bacteria.

Although the SERS enhancement from an isolated spherical nanoparticle is not as large as nanoparticle aggregates, there are anisotropic nanoparticles that offer a large SERS enhancement similar to spherical nanoparticle aggregates. Examples include nanostars, spiked beads, nanocubes, nanorods, octahedral structured nanoparticles, and nanoantenna, to list few [87-97]. All the listed nanoparticles, with the appropriate functionalization, can be used as SERS probes for imaging cell membrane proteins. For example, Wark and coworkers used Raman reporters encapsulated onto gold nanorods with a polyelectrolyte coating for imaging dendritic cells [90].

They adsorbed three different Raman reporters (diethyl-2,20-cyanine iodide, diethylthiadicarbocyanine iodide and IR1048) on a single nanorod to develop universal Raman probes that can be imaged with commonly available lasers across the wavelength region of 512 nm to 1064 nm. The polymer coating on these universal tags can be functionalized with appropriate ligand or antibody for imaging cell membrane proteins.

Nanoshell and nanogap-containing nanoparticles are another type of material used as SERS probes. Isolated nanoshells (*i.e.*, a dielectric material surrounded by a metal shell) have been shown to be capable of producing similar SERS signals of nanosphere dimers, circumventing the need to produce SERS probes with precisely defined aggregation [98]. Guo and coworkers reported that nanoshells consisting of silica-embedded Raman reporter (RuBPy) with a gold coating produce a SERS enhancement on the order of 10^{11} to 10^{14} [99]. Singamaneni and coworkers have reported a Raman reporter placed in a gap between a gold core and a gold shell (termed BRIGHTs) generates a twenty-fold SERS enhancement compared to similarly sized gold nanopopcorn [100]. They functionalized the BRIGHTs surface with ERbB2 antibody to image ERbB2 receptor on the surface of SKBR-3 cells. Similarly, in 2016, He and coworkers reported uniform nanogap-containing gold core and shell particles that are formed due to polyadenine spacers [101]. The SERS enhancement was sensitive to the size of the metal core. A Raman reporter such as 4,4'-dipyridyl and 5,5'-dithiobis(2-nitrobenzoin acid) was placed in the nanogaps, and the particle surface was functionalized to image CD44 receptors on tumor cells.

As previously stated in the introduction, Raman imaging has benefits over fluorescence for multiplexing. Raman imaging is ideal for mapping multiple protein biomarkers on the cell membrane, which is often necessary for accurate diagnosis, disease staging and selecting therapeutic interventions [10, 102, 103]. SERS or SERRS probes have been used for imaging three

to four proteins simultaneously in the cell membrane [104-106]. Liz-Marzan and coworkers reported poly(N-isopropylacrylamide) microgel-encapsulated gold octahedral nanoparticles loaded with three different Raman reporters to image tumor-associated biomarkers: epidermal growth factor receptor (EGFR), epithelial cell adhesion molecule (EpCAM) and homing cell adhesion molecule (CD44) [107]. They were able to successfully discriminate between tumor and nontumor cells. This and other proof-of-concept studies support the possibility of even higher levels of multiplexing with Raman imaging.

2.3. Tip-Enhanced Raman Scattering

Tip-enhanced Raman spectroscopy (TERS) provides nanometer spatial resolution by combining SERS and scanning probe microscopies such as atomic force microscopy (AFM), scanning tunneling microscopy (STM) or shear-force microscopy (SFM). Immediately after STM was realized in 1985, Wessel proposed an idea of "Surface-enhanced optical microscopy" [108]. Fifteen years later, several groups reported TERS with an AFM tip [109-111]. The basic idea is a sharp metal or metal-coated tip is placed near (in the near field) to the sample surface, which generates a SERS-type effect that is localized to a spatial scale typically on the order of 10 nm to 20 nm [112]. A spatial resolution of 0.5 nm was reported for TERS of a single porphyrin molecule adsorbed on a silver surface [113]. The TERS enhancement is dependent on the distance between the sample and the tip (the enhancement decays exponentially), polarization of the incident radiation, shape and the material of the metal or nanoparticle on the tip [114-118]. In comparison to AFM-based TERS, STM offers better control of the distance between the tip and sample, which

is a critical parameter [119]. However, for STM-based TERS either the sample needs to be conductive or an extremely thin sample must be on a metal substrate.

As a surface sensitive technique with nanometer spatial resolution, TERS is a valuable tool for label-free chemical imaging of lipid bilayers and the cell membrane. TERS has been extensively used for the chemical analysis of model lipid membrane composition and nanometer-scale domains [120-122]. In 2009, Deckert and coworkers used AFM-based TERS to analyze the surface of the human cell line HaCaT at a spatial resolution of 10 nm [123]. They used supported lipid bilayers as a model system to interpret the complex TERS spectrum from the cells. In another study, the same group used TERS to characterize protein and lipids in the bilayer at nanometer spatial resolution [124]. Three types of domains were identified corresponding to lipid-only, protein-only and lipid-protein domains. In another study by the same group , human colon-cancer cells were used as a model to analyze by TERS nanometer-sized protein-rich and lipid-rich domains [122]. Schultz and coworkers used RGD ligand-coated nanoparticles to specifically image integrins in the intact cell membrane by TERS [125-127]. They measured similar spectra for the receptors in the cell membrane and for purified receptor. They were able to differentiate two different integrins ($\alpha5\beta1$ and $\alpha v\beta3$) on the cell surface.

TERS has been applied to study the chemical composition of the cell surface of microorganisms, such as bacteria. Popp and coworkers studied the cell membrane of the gram-positive bacteria with TERS at a 50 nm spatial resolution [128]. The recorded TERS spectrum primarily consists of peaks corresponding to peptides and polysaccharides. In a follow-up study, TERS in combination with infrared absorption, micro-Raman spectroscopy and UV resonance Raman spectroscopy was used for the detailed chemical analysis of metabolism in gram-positive bacteria [129]. In this study, TERS was specifically used for probing structure and dynamics of

polysaccharide and peptide components on the bacterial cell membrane. TERS has also been used to study the surface of virus particles. The coat proteins on the surface of the tobacco mosaic virus were analyzed with a spatial resolution less than 50 nm [130]. Naumann and coworkers characterized different virus strains based on their TERS spectral signature [131]. Very recently, Popp and coworkers have discriminated different viruses using TERS and chemometrics [132].

The selected examples presented here show that TERS is a valuable tool for the chemical analysis of the cell membrane with a spatial resolution of a few tens of nanometers. Although TERS experiments have up to now primarily focused on fixed samples, improvements in the acquisition speed will enable the analysis of the dynamic processes in live cells. Van Duyne and coworkers have shown that by coupling TERS to ultrafast spectroscopy, the temporal resolution in TERS can be improved [133].

3. EXOGENOUS SMALL MOLECULE AND MULTICOLOR TAGS FOR SPECIFIC LABELING

Although label-free Raman imaging is a powerful technique for the chemical analysis of the cell membrane, the identity of a specific protein or a lipid is lost in the ensemble signal. Labeling a specific protein or lipid is sometimes desired, as highlighted by several of the examples discussed above. Properly engineered SERS probes have general utility for adding selectivity to the Raman measurement. However, the size of many SERS probes could be too invasive for some measurements. In this section, specialized small Raman tags (as small as two atoms) that have Raman peaks in the cell-silent region are discussed. Although the Raman signal corresponding to

these tags may not be as large as measured for SERS probes, the Raman peak location in the cell-silent region makes them highly advantageous for selective labeling. The research in this area is developing, and most of the experiments discussed here are proof of concept. These tags are expected to play a significant role in Raman imaging of the cell membrane.

These Raman tags are borrowed from the popular biorthogonal tags for fluorescence imaging. In a typical bioorthogonal labeling experiment, a small alkyne (C≡C) or azide (N_3) tag is introduced as a handle into the species of interest, such as lipids and proteins in live cells. For fluorescence, the inserted handle is further used for attaching a label for detection [134]. The success of this approach is attributed to the incorporation of the handle with minimum perturbation to any endogenous activity in the cellular environment. In this regard, the Cu-catalyzed click chemistry is a well utilized chemical reaction [135, 136]. However, the installation of a fluorescent label by Cu-catalyzed click chemistry is limited to fixed cells or cell lysate due to the toxicity of the metal catalyzed reaction. Bertozzi and co-workers developed a Cu-free version of click chemistry using highly strained molecules that promote the chemical reaction in the absence of catalyst in live cells [137]. However, the reaction kinetics are slow. All these limitations of bio-orthogonal chemistry can be avoided in Raman imaging by measuring the signal from the handle itself without the need of using click chemistry to introduce a fluorophore.

The characteristic Raman signal corresponding to alkyne or azide tags appears in the cell-silent region. Sodeka and coworkers reported the spontaneous line-scanning Raman imaging of alkyne-tagged 2-deoxyuridine (EdU) at 2122 cm^{-1} in live HeLa cells [138]. The EdU is used as a cell proliferation probe. The Raman signal mainly originates from the cell nucleus due to binding of EdU to newly synthesized DNA. In a follow-up study, the authors reported various small alkynes, nitrile (C≡N) and deuterium (C-D) tags that can be used for Raman imaging in the range

of 2084cm^{-1} to 2258 cm^{-1} [139]. Further, all tags were characterized for their Raman intensity compared to the originally reported EdU tag. In all cases, the alkyne tags have higher intensity compared to the nitrile and deuterium-derived tags. As a demonstration study of cellular uptake and accumulation of small molecules, the alkyne-labeled coenzyme Q (CoQ) lipid analogs of varying hydrophobicities were measured in HeLa cells. The cellular uptake and localization of CoQ analogues measured by Raman imaging were observed to be dependent on the hydrophobicity of the CoQ. Further, using two different alkyne tags to label DNA and CoQ, multiplexed imaging has been done in HeLa cells to separate the signal at 2122 cm^{-1}and 2248 cm^{-1} from the nucleus and cytoplasm, respectively.

Alkyne, nitrile, and deuterium tags are useful as small exogenous Raman tags for labeling cell membrane components for spontaneous Raman imaging, although higher signals can be obtained with these tags using stimulated Raman scattering (SRS). Min and coworkers reported the implementation of SRS for imaging the C-D bond in a deuterated sample [58]. SRS was used rather than CARS due to the lower background and straightforward interpretation of the SRS signal. Deuterated leucine was used as a precursor for protein synthesis in HeLa cells. The spatial distribution of the protein signal was similar to the signal observed in bio-orthogonal measurements through fluorescence detection in fixed cells. The observed signal was decreased when protein synthesis-inhibiting drugs were used, indicating the origin of the C-D signal was from protein synthesis. This approach was also applied to image protein distribution in HEK293T and neural cells at physiological conditions [58]. The signal was amplified many fold by using a deuterated derivative of all amino acids as the precursors. As shown in Figure 4i-l, the authors were able to monitor the time-dependent *de novo* protein synthesis at 5 hours (Figure 4i) and at 20 hours (Figure 4k) after introducing deuterium labeled amino acids in HeLa cells. SRS was used to

image the synthesis of DNA, RNA, proteomes, phospholipids and triglycerides in live cells using alkyne tags [140]. In 2016, Potma and coworkers used deuterated cholesterol as a Raman-active probe to measure cholesterol storage in lipid droplets in cells [141]. Further, Li *et al.*, measured lipogenesis in live cells using deuterated glucose as a Raman-active probe (Figure 4m-n) [57]. Diyne-derived cholesterol was used to measure cholesterol storage in live CHO cells with SRS (Figure 4o-p) [60].

Alkyne structures with variable substitution were reported for dual-color Raman imaging with spontaneous Raman imaging. However, most of the alkyne structures that can be multiplexed over two colors have overlapping peaks. In 2014, Min and coworkers reported that by replacing ^{12}C in the simplest alkyne (C≡C) with one ^{13}C or two ^{13}C through isotope replacement, alkyne tags with three distinct signals at 2048, 2077 and 2125 cm^{-1} could be easily resolved [142]. As a proof of concept for multiplexing, lipids, DNA and RNA were successfully mapped in a single HeLa cell with minimum cross talk among the detection channels. Another advantage for using isotope labeled alkyne is that all color tags are chemically identical, hence there are fewer differences in the perturbation from the tag structure. Very recently, alkyne-tags coupled with SERS probes were used for three color Raman imaging in the 2100 to 2300 cm^{-1} region [143]. As shown in Figure 5, these hybrid probes were used to image folic acid receptor and luteinizing hormone-releasing hormone receptor on the HeLa cell membrane.

Multicolor Raman imaging can be performed using carbon nanotubes (CNT). CNTs provide unique optical properties, including resonance with near-infrared excitation. The CNT are serum-stable and have minimum cytotoxicity with suitable surface functionalization [144]. The surface of the CNT can be easily functionalized to target a specific protein on the cell membrane [145]. The Raman band corresponding to CNT is very sharp, which makes them suitable for

multiplexed Raman imaging. As a proof of concept, Dai and coworkers showed that up to three color imaging can be performed with CNT in fixed cancer cells by modulating the $^{13}C/^{12}C$ isotope composition [146]. They measured three membrane proteins including epidermal growth factor receptor, integrins and receptor tyrosine-protein kinase ErbB-2. In a follow-up study, they increased the number of targeted receptors to five (Figure 6) [147].

4. CONCLUSIONS AND OUTLOOK

The Raman signal encodes the identity of the functional groups within the molecule and thus enables label-free chemical imaging. Coherent Raman scattering, tip enhanced Raman scattering and surface enhanced Raman scattering are common Raman imaging modalities for lipid and cell membrane studies. The highlighted advantages of each of these techniques are varied in relation to cell membrane studies. The coherent nature of the Raman signal allows video-rate chemical imaging of lipids and proteins with CARS and SRS, and the demonstrations of improved spatial resolution CARS and SRS imaging with non-biological samples may be extended to biological studies in the near future. The SERS signal can parallel the fluorescence signal intensity, and multiple membrane proteins on the cell membrane have been specifically imaged with Raman reporter-encapsulated SERS probes. Cell membrane components have been analyzed with a spatial resolution around 10 nm with TERS, and methods to improve imaging speed with TERS are being reported. The utility of all these techniques is expanded with tags, such as alkyne, deuterium or azide, to generate a signal in the cell-silent region that is free of cellular background and extends Raman multiplexing. Several exciting prospects for cell membrane studies include subdiffraction, video rate CARS and SRS imaging of cell membrane components, which would aid studies of

membrane dynamics. Similarly, the ability to combine multiplexed SERS measurements with membrane protein tracking would enable the simultaneous measurement of the diffusion of multiple membrane proteins. Finally, future applications of Raman imaging will benefit from the labeling of a specific membrane protein with a unique Raman tag either genetically or endogenously.

DISCLOSURE STATEMENT

The authors are not aware of any affiliations, memberships, funding, or financial holdings that might be perceived as affecting the objectivity of this review.

ACKNOWLEDGEMENTS

The authors thank National Science Foundation (CHE-1412084) for financial support and Ms. Qiaochu Zhu and Professor Jacob W. Petrich for helpful discussion.

LITERATURE CITED

[1] S.J. Singer, G.L. Nicolson, The fluid mosaic model of the structure of cell membranes, Science, 175 (1972) 720-731.
[2] D.M. Engelman, Membranes are more mosaic than fluid, Nature, 438 (2005) 578-580.
[3] A. Kusumi, I. Koyama-Honda, K. Suzuki, Molecular Dynamics and Interactions for Creation of Stimulation-Induced Stabilized Rafts from Small Unstable Steady-State Rafts, Traffic, 5 (2004) 213-230.
[4] G.L. Nicolson, Transmembrane control of the receptors on normal and tumor cells, Biochimica et Biophysica Acta (BBA) - Reviews on Biomembranes, 457 (1976) 57-108.
[5] A. Kusumi, C. Nakada, K. Ritchie, K. Murase, K. Suzuki, H. Murakoshi, R.S. Kasai, J. Kondo, T. Fujiwara, Paradigm Shift of the Plasma Membrane Concept from the Two-Dimensional Continuum Fluid to the Partitioned Fluid: High-Speed Single-Molecule Tracking of Membrane Molecules, Annual Review of Biophysics and Biomolecular Structure, 34 (2005) 351-378.
[6] E.J. Luna, A.L. Hitt, Cytoskeleton--plasma membrane interactions, Science, 258 (1992) 955-964.
[7] A. Watts, Membrane structure and dynamics, Current Opinion in Cell Biology, 1 (1989) 691-700.
[8] G.L. Nicolson, The Fluid-Mosaic Model of Membrane Structure: still relevant to understanding the structure, function and dynamics of biological membranes after more than 40 years, Biochim Biophys Acta, 1838 (2014) 1451-1466.
[9] F.R. Maxfield, I. Tabas, Role of cholesterol and lipid organization in disease, Nature, 438 (2005) 612-621.
[10] R. Leth-Larsen, R.R. Lund, H.J. Ditzel, Plasma membrane proteomics and its application in clinical cancer biomarker discovery, Mol Cell Proteomics, 9 (2010) 1369-1382.
[11] C.V. Raman, K.S. Krishnan, A New Type of Secondary Radiation, Nature, 121 (1928) 501-502.
[12] Q. Matthews, A.G. Brolo, J. Lum, X. Duan, A. Jirasek, Raman spectroscopy of single human tumour cells exposed to ionizing radiationin vitro, Physics in Medicine and Biology, 56 (2011) 19-38.
[13] J. Ando, A.F. Palonpon, M. Sodeoka, K. Fujita, High-speed Raman imaging of cellular processes, Current Opinion in Chemical Biology, 33 (2016) 16-24.
[14] S. Stewart, R.J. Priore, M.P. Nelson, P.J. Treado, Raman Imaging, Annual Review of Analytical Chemistry, 5 (2012) 337-360.
[15] L. Opilik, T. Schmid, R. Zenobi, Modern Raman Imaging: Vibrational Spectroscopy on the Micrometer and Nanometer Scales, Annual Review of Analytical Chemistry, 6 (2013) 379-398.
[16] H.J. Butler, L. Ashton, B. Bird, G. Cinque, K. Curtis, J. Dorney, K. Esmonde-White, N.J. Fullwood, B. Gardner, P.L. Martin-Hirsch, M.J. Walsh, M.R. McAinsh, N. Stone, F.L. Martin, Using Raman spectroscopy to characterize biological materials, Nature Protocols, 11 (2016) 664-687.
[17] R.W. Terhune, P.D. Maker, C.M. Savage, Measurements of Nonlinear Light Scattering, Physical Review Letters, 14 (1965) 681-684.
[18] M.D. Duncan, J. Reintjes, T.J. Manuccia, Scanning coherent anti-Stokes Raman microscope, Optics Letters, 7 (1982) 350.
[19] A. Zumbusch, G.R. Holtom, X.S. Xie, Three-Dimensional Vibrational Imaging by Coherent Anti-Stokes Raman Scattering, Physical Review Letters, 82 (1999) 4142-4145.

[20] C.L. Evans, E.O. Potma, M. Puoris'haag, D. Cote, C.P. Lin, X.S. Xie, Chemical imaging of tissue in vivo with video-rate coherent anti-Stokes Raman scattering microscopy, Proceedings of the National Academy of Sciences, 102 (2005) 16807-16812.
[21] A. Volkmer, J.-X. Cheng, X. Sunney Xie, Vibrational Imaging with High Sensitivity via Epidetected Coherent Anti-Stokes Raman Scattering Microscopy, Physical Review Letters, 87 (2001).
[22] C.L. Evans, X.S. Xie, Coherent Anti-Stokes Raman Scattering Microscopy: Chemical Imaging for Biology and Medicine, Annual Review of Analytical Chemistry, 1 (2008) 883-909.
[23] J.-X. Cheng, X.S. Xie, Coherent Anti-Stokes Raman Scattering Microscopy: Instrumentation, Theory, and Applications, The Journal of Physical Chemistry B, 108 (2004) 827-840.
[24] M. Müller, A. Zumbusch, Coherent anti-Stokes Raman Scattering Microscopy, Chemphyschem, 8 (2007) 2156-2170.
[25] F. El-Diasty, Coherent anti-Stokes Raman scattering: Spectroscopy and microscopy, Vibrational Spectroscopy, 55 (2011) 1-37.
[26] J.X. Cheng, X.S. Xie, Vibrational spectroscopic imaging of living systems: An emerging platform for biology and medicine, Science, 350 (2015) aaa8870-aaa8870.
[27] B.G. Saar, C.W. Freudiger, J. Reichman, C.M. Stanley, G.R. Holtom, X.S. Xie, Video-Rate Molecular Imaging in Vivo with Stimulated Raman Scattering, Science, 330 (2010) 1368-1370.
[28] M. Müller, J.M. Schins, Imaging the Thermodynamic State of Lipid Membranes with Multiplex CARS Microscopy, The Journal of Physical Chemistry B, 106 (2002) 3715-3723.
[29] H.A. Rinia, K.N.J. Burger, M. Bonn, M. Müller, Quantitative Label-Free Imaging of Lipid Composition and Packing of Individual Cellular Lipid Droplets Using Multiplex CARS Microscopy, Biophysical Journal, 95 (2008) 4908-4914.
[30] G.W.H. Wurpel, J.M. Schins, M. Müller, Chemical specificity in three-dimensional imaging with multiplex coherent anti-Stokes Raman scattering microscopy, Optics Letters, 27 (2002) 1093.
[31] C. Jüngst, M.J. Winterhalder, A. Zumbusch, Fast and long term lipid droplet tracking with CARS microscopy, Journal of Biophotonics, 4 (2011) 435-441.
[32] J.-X. Cheng, Y.K. Jia, G. Zheng, X.S. Xie, Laser-Scanning Coherent Anti-Stokes Raman Scattering Microscopy and Applications to Cell Biology, Biophysical Journal, 83 (2002) 502-509.
[33] H. Kano, Molecular vibrational imaging of a human cell by multiplex coherent anti-Stokes Raman scattering microspectroscopy using a supercontinuum light source, Journal of Raman Spectroscopy, 39 (2008) 1649-1652.
[34] Y. Fu, H. Wang, T.B. Huff, R. Shi, J.X. Cheng, Coherent anti-Stokes Raman scattering imaging of myelin degradation reveals a calcium-dependent pathway in lyso-PtdCho-induced demyelination, J Neurosci Res, 85 (2007) 2870-2881.
[35] J. Imitola, D. Cote, S. Rasmussen, X.S. Xie, Y. Liu, T. Chitnis, R.L. Sidman, C.P. Lin, S.J. Khoury, Multimodal coherent anti-Stokes Raman scattering microscopy reveals microglia-associated myelin and axonal dysfunction in multiple sclerosis-like lesions in mice, J Biomed Opt, 16 (2011) 021109.
[36] E. Belanger, F.P. Henry, R. Vallee, M.A. Randolph, I.E. Kochevar, J.M. Winograd, C.P. Lin, D. Cote, In vivo evaluation of demyelination and remyelination in a nerve crush injury model, Biomed Opt Express, 2 (2011) 2698-2708.
[37] H.-W. Wang, T.T. Le, J.-X. Cheng, Label-free imaging of arterial cells and extracellular matrix using a multimodal CARS microscope, Optics Communications, 281 (2008) 1813-1822.

[38] A. Pliss, A.N. Kuzmin, A.V. Kachynski, P.N. Prasad, Nonlinear Optical Imaging and Raman Microspectrometry of the Cell Nucleus throughout the Cell Cycle, Biophysical Journal, 99 (2010) 3483-3491.
[39] X. Nan, Vibrational imaging of lipid droplets in live fibroblast cells with coherent anti-Stokes Raman scattering microscopy, The Journal of Lipid Research, 44 (2003) 2202-2208.
[40] X. Nan, E.O. Potma, X.S. Xie, Nonperturbative Chemical Imaging of Organelle Transport in Living Cells with Coherent Anti-Stokes Raman Scattering Microscopy, Biophysical Journal, 91 (2006) 728-735.
[41] R.K. Lyn, D.C. Kennedy, A. Stolow, A. Ridsdale, J.P. Pezacki, Dynamics of lipid droplets induced by the hepatitis C virus core protein, Biochemical and Biophysical Research Communications, 399 (2010) 518-524.
[42] D.A. Brown, E. London, Functions of lipid rafts in biological membranes, Annu Rev Cell Dev Biol, 14 (1998) 111-136.
[43] L.J. Pike, Lipid rafts: bringing order to chaos, J Lipid Res, 44 (2003) 655-667.
[44] G.W.H. Wurpel, J.M. Schins, M. Müller, Direct Measurement of Chain Order in Single Phospholipid Mono- and Bilayers with Multiplex CARS, The Journal of Physical Chemistry B, 108 (2004) 3400-3403.
[45] E.O. Potma, X.S. Xie, Direct Visualization of Lipid Phase Segregation in Single Lipid Bilayers with Coherent Anti-Stokes Raman Scattering Microscopy, Chemphyschem, 6 (2005) 77-79.
[46] L. Li, H. Wang, J.-X. Cheng, Quantitative Coherent Anti-Stokes Raman Scattering Imaging of Lipid Distribution in Coexisting Domains, Biophysical Journal, 89 (2005) 3480-3490.
[47] Li, J.-X. Cheng, Label-Free Coherent Anti-Stokes Raman Scattering Imaging of Coexisting Lipid Domains in Single Bilayers, The Journal of Physical Chemistry B, 112 (2008) 1576-1579.
[48] D. Zhang, P. Wang, M.N. Slipchenko, J.-X. Cheng, Fast Vibrational Imaging of Single Cells and Tissues by Stimulated Raman Scattering Microscopy, Accounts of Chemical Research, 47 (2014) 2282-2290.
[49] D. Fu, F.-K. Lu, X. Zhang, C. Freudiger, D.R. Pernik, G. Holtom, X.S. Xie, Quantitative Chemical Imaging with Multiplex Stimulated Raman Scattering Microscopy, Journal of the American Chemical Society, 134 (2012) 3623-3626.
[50] Jeffrey L. Suhalim, C.-Y. Chung, Magnus B. Lilledahl, Ryan S. Lim, M. Levi, Bruce J. Tromberg, Eric O. Potma, Characterization of Cholesterol Crystals in Atherosclerotic Plaques Using Stimulated Raman Scattering and Second-Harmonic Generation Microscopy, Biophysical Journal, 102 (2012) 1988-1995.
[51] D. Zhang, P. Wang, M.N. Slipchenko, D. Ben-Amotz, A.M. Weiner, J.-X. Cheng, Quantitative Vibrational Imaging by Hyperspectral Stimulated Raman Scattering Microscopy and Multivariate Curve Resolution Analysis, Analytical Chemistry, 85 (2013) 98-106.
[52] X. Zhang, M.B.J. Roeffaers, S. Basu, J.R. Daniele, D. Fu, C.W. Freudiger, G.R. Holtom, X.S. Xie, Label-Free Live-Cell Imaging of Nucleic Acids Using Stimulated Raman Scattering Microscopy, Chemphyschem, 13 (2012) 1054-1059.
[53] S. Yue, J. Li, S.Y. Lee, H.J. Lee, T. Shao, B. Song, L. Cheng, T.A. Masterson, X. Liu, T.L. Ratliff, J.X. Cheng, Cholesteryl ester accumulation induced by PTEN loss and PI3K/AKT activation underlies human prostate cancer aggressiveness, Cell Metab, 19 (2014) 393-406.
[54] M.N. Slipchenko, T.T. Le, H. Chen, J.-X. Cheng, High-Speed Vibrational Imaging and Spectral Analysis of Lipid Bodies by Compound Raman Microscopy, The Journal of Physical Chemistry B, 113 (2009) 7681-7686.

[55] D. Zhang, M.N. Slipchenko, J.-X. Cheng, Highly Sensitive Vibrational Imaging by Femtosecond Pulse Stimulated Raman Loss, The Journal of Physical Chemistry Letters, 2 (2011) 1248-1253.
[56] C.-S. Liao, M.N. Slipchenko, P. Wang, J. Li, S.-Y. Lee, R.A. Oglesbee, J.-X. Cheng, Microsecond scale vibrational spectroscopic imaging by multiplex stimulated Raman scattering microscopy, Light: Science & Applications, 4 (2015) e265.
[57] J. Li, J.-X. Cheng, Direct Visualization of De novo Lipogenesis in Single Living Cells, Scientific Reports, 4 (2014) 6807.
[58] L. Wei, Y. Yu, Y. Shen, M.C. Wang, W. Min, Vibrational imaging of newly synthesized proteins in live cells by stimulated Raman scattering microscopy, Proceedings of the National Academy of Sciences, 110 (2013) 11226-11231.
[59] F. Hu, L. Wei, C. Zheng, Y. Shen, W. Min, Live-cell vibrational imaging of choline metabolites by stimulated Raman scattering coupled with isotope-based metabolic labeling, The Analyst, 139 (2014) 2312.
[60] H.J. Lee, W. Zhang, D. Zhang, Y. Yang, B. Liu, E.L. Barker, K.K. Buhman, L.V. Slipchenko, M. Dai, J.-X. Cheng, Assessing Cholesterol Storage in Live Cells and C. elegans by Stimulated Raman Scattering Imaging of Phenyl-Diyne Cholesterol, Scientific Reports, 5 (2015) 7930.
[61] H. Kim, G.W. Bryant, S.J. Stranick, Superresolution four-wave mixing microscopy, Optics Express, 20 (2012) 6042.
[62] P. Wang, M.N. Slipchenko, J. Mitchell, C. Yang, E.O. Potma, X. Xu, J.-X. Cheng, Far-field imaging of non-fluorescent species with subdiffraction resolution, Nature Photonics, 7 (2013) 449-453.
[63] W.R. Silva, C.T. Graefe, R.R. Frontiera, Toward Label-Free Super-Resolution Microscopy, ACS Photonics, 3 (2016) 79-86.
[64] P. Hildebrandt, M. Stockburger, Surface-enhanced resonance Raman spectroscopy of Rhodamine 6G adsorbed on colloidal silver, The Journal of Physical Chemistry, 88 (1984) 5935-5944.
[65] J.A. Creighton, C.G. Blatchford, M.G. Albrecht, Plasma resonance enhancement of Raman scattering by pyridine adsorbed on silver or gold sol particles of size comparable to the excitation wavelength, Journal of the Chemical Society, Faraday Transactions 2, 75 (1979) 790.
[66] K.C. Grabar, K.R. Brown, C.D. Keating, S.J. Stranick, S.-L. Tang, M.J. Natan, Nanoscale Characterization of Gold Colloid Monolayers: A Comparison of Four Techniques, Analytical Chemistry, 69 (1997) 471-477.
[67] C.G. Blatchford, J.R. Campbell, J.A. Creighton, Plasma resonance — enhanced raman scattering by absorbates on gold colloids: The effects of aggregation, Surface Science, 120 (1982) 435-455.
[68] A.C. Curtis, D.G. Duff, P.P. Edwards, D.A. Jefferson, B.F.G. Johnson, A.I. Kirkland, A.S. Wallace, Preparation and structural characterization of an unprotected copper sol, The Journal of Physical Chemistry, 92 (1988) 2270-2275.
[69] H.H. Huang, F.Q. Yan, Y.M. Kek, C.H. Chew, G.Q. Xu, W. Ji, P.S. Oh, S.H. Tang, Synthesis, Characterization, and Nonlinear Optical Properties of Copper Nanoparticles, Langmuir, 13 (1997) 172-175.
[70] M. Moskovits, Surface-enhanced spectroscopy, Reviews of Modern Physics, 57 (1985) 783-826.
[71] M. Moskovits, Persistent misconceptions regarding SERS, Physical Chemistry Chemical Physics, 15 (2013) 5301.

[72] G. McNay, D. Eustace, W.E. Smith, K. Faulds, D. Graham, Surface-enhanced Raman scattering (SERS) and surface-enhanced resonance Raman scattering (SERRS): a review of applications, Appl Spectrosc, 65 (2011) 825-837.
[73] A. Pallaoro, G.B. Braun, M. Moskovits, Biotags Based on Surface-Enhanced Raman Can Be as Bright as Fluorescence Tags, Nano Letters, 15 (2015) 6745-6750.
[74] G. Sabatté, R. Keir, M. Lawlor, M. Black, D. Graham, W.E. Smith, Comparison of Surface-Enhanced Resonance Raman Scattering and Fluorescence for Detection of a Labeled Antibody, Analytical Chemistry, 80 (2008) 2351-2356.
[75] G. Goddard, L.O. Brown, R. Habbersett, C.I. Brady, J.C. Martin, S.W. Graves, J.P. Freyer, S.K. Doorn, High-Resolution Spectral Analysis of Individual SERS-Active Nanoparticles in Flow, Journal of the American Chemical Society, 132 (2010) 6081-6090.
[76] X.X. Han, H.Y. Jia, Y.F. Wang, Z.C. Lu, C.X. Wang, W.Q. Xu, B. Zhao, Y. Ozaki, Analytical Technique for Label-Free Multi-Protein Detection Based on Western Blot and Surface-Enhanced Raman Scattering, Analytical Chemistry, 80 (2008) 2799-2804.
[77] I. Pavel, E. McCarney, A. Elkhaled, A. Morrill, K. Plaxco, M. Moskovits, Label-Free SERS Detection of Small Proteins Modified to Act as Bifunctional Linkers, The Journal of Physical Chemistry C, 112 (2008) 4880-4883.
[78] D. Zanchet, C.M. Micheel, W.J. Parak, D. Gerion, S.C. Williams, A.P. Alivisatos, Electrophoretic and Structural Studies of DNA-Directed Au Nanoparticle Groupings, The Journal of Physical Chemistry B, 106 (2002) 11758-11763.
[79] J.I.L. Chen, Y. Chen, D.S. Ginger, Plasmonic Nanoparticle Dimers for Optical Sensing of DNA in Complex Media, Journal of the American Chemical Society, 132 (2010) 9600-9601.
[80] L. Fabris, M. Dante, T.-Q. Nguyen, J.B.H. Tok, G.C. Bazan, SERS Aptatags: New Responsive Metallic Nanostructures for Heterogeneous Protein Detection by Surface Enhanced Raman Spectroscopy, Advanced Functional Materials, 18 (2008) 2518-2525.
[81] A.S.D.S. Indrasekara, B.J. Paladini, D.J. Naczynski, V. Starovoytov, P.V. Moghe, L. Fabris, Dimeric Gold Nanoparticle Assemblies as Tags for SERS-Based Cancer Detection, Advanced Healthcare Materials, 2 (2013) 1370-1376.
[82] D. Chen, H. Feng, J. Li, Graphene Oxide: Preparation, Functionalization, and Electrochemical Applications, Chemical Reviews, 112 (2012) 6027-6053.
[83] Z. Liu, Z. Guo, H. Zhong, X. Qin, M. Wan, B. Yang, Graphene oxide based surface-enhanced Raman scattering probes for cancer cell imaging, Physical Chemistry Chemical Physics, 15 (2013) 2961.
[84] J. Huang, C. Zong, H. Shen, M. Liu, B. Chen, B. Ren, Z. Zhang, Mechanism of Cellular Uptake of Graphene Oxide Studied by Surface-Enhanced Raman Spectroscopy, Small, 8 (2012) 2577-2584.
[85] Q. Liu, L. Wei, J. Wang, F. Peng, D. Luo, R. Cui, Y. Niu, X. Qin, Y. Liu, H. Sun, J. Yang, Y. Li, Cell imaging by graphene oxide based on surface enhanced Raman scattering, Nanoscale, 4 (2012) 7084-7089.
[86] D. Lin, T. Qin, Y. Wang, X. Sun, L. Chen, Graphene Oxide Wrapped SERS Tags: Multifunctional Platforms toward Optical Labeling, Photothermal Ablation of Bacteria, and the Monitoring of Killing Effect, ACS Applied Materials & Interfaces, 6 (2014) 1320-1329.
[87] L. Rodríguez-Lorenzo, R.n.A. Álv rez-Puebla, I. Pastoriza-Santos, S. Mazzucco, O. Stéph n, M. Kociak, L.M. Liz-Marzán, F.J. García de Abajo, Zeptomol Detection Through Controlled Ultrasensitive Surface-Enhanced Raman Scattering, Journal of the American Chemical Society, 131 (2009) 4616-4618.

[88] P. Aldeanueva-Potel, E. Carbo-Argibay, N. Pazos-Perez, S. Barbosa, I. Pastoriza-Santos, R.A. Alvarez-Puebla, L.M. Liz-Marzan, Spiked gold beads as substrates for single-particle SERS, Chemphyschem, 13 (2012) 2561-2565.
[89] M. Rycenga, P.H.C. Camargo, W. Li, C.H. Moran, Y. Xia, Understanding the SERS Effects of Single Silver Nanoparticles and Their Dimers, One at a Time, The Journal of Physical Chemistry Letters, 1 (2010) 696-703.
[90] A. McLintock, C.A. Cunha-Matos, M. Zagnoni, O.R. Millington, A.W. Wark, Universal Surface-Enhanced Raman Tags: Individual Nanorods for Measurements from the Visible to the Infrared (514–1064 nm), ACS Nano, 8 (2014) 8600-8609.
[91] M.J. Mulvihill, X.Y. Ling, J. Henzie, P. Yang, Anisotropic Etching of Silver Nanoparticles for Plasmonic Structures Capable of Single-Particle SERS, Journal of the American Chemical Society, 132 (2010) 268-274.
[92] S.L. Kleinman, B. Sharma, M.G. Blaber, A.-I. Henry, N. Valley, R.G. Freeman, M.J. Natan, G.C. Schatz, R.P. Van Duyne, Structure Enhancement Factor Relationships in Single Gold Nanoantennas by Surface-Enhanced Raman Excitation Spectroscopy, Journal of the American Chemical Society, 135 (2013) 301-308.
[93] H. Liang, Z. Li, W. Wang, Y. Wu, H. Xu, Highly Surface-roughened â□œFlower-likeâ€• Silver Nanoparticles for Extremely Sensitive Substrates of Surface-enhanced Raman Scattering, Advanced Materials, 21 (2009) 4614-4618.
[94] D. Steinigeweg, M. Schütz, S. Schlücker, Single gold trimers and 3D superstructures exhibit a polarization-independent SERS response, Nanoscale, 5 (2013) 110-113.
[95] M. Rycenga, X. Xia, C.H. Moran, F. Zhou, D. Qin, Z.-Y. Li, Y. Xia, Generation of Hot Spots with Silver Nanocubes for Single-Molecule Detection by Surface-Enhanced Raman Scattering, Angewandte Chemie International Edition, 50 (2011) 5473-5477.
[96] H.X. Lin, J.M. Li, B.J. Liu, D.Y. Liu, J. Liu, A. Terfort, Z.X. Xie, Z.Q. Tian, B. Ren, Uniform gold spherical particles for single-particle surface-enhanced Raman spectroscopy, Phys Chem Chem Phys, 15 (2013) 4130-4135.
[97] H. Yuan, Y. Liu, A.M. Fales, Y.L. Li, J. Liu, T. Vo-Dinh, Quantitative Surface-Enhanced Resonant Raman Scattering Multiplexing of Biocompatible Gold Nanostars for in Vitro and ex Vivo Detection, Analytical Chemistry, 85 (2013) 208-212.
[98] C.E. Talley, J.B. Jackson, C. Oubre, N.K. Grady, C.W. Hollars, S.M. Lane, T.R. Huser, P. Nordlander, N.J. Halas, Surface-Enhanced Raman Scattering from Individual Au Nanoparticles and Nanoparticle Dimer Substrates, Nano Letters, 5 (2005) 1569-1574.
[99] P. Zhang, Y. Guo, Surface-Enhanced Raman Scattering inside Metal Nanoshells, Journal of the American Chemical Society, 131 (2009) 3808-3809.
[100] N. Gandra, S. Singamaneni, Bilayered Raman-Intense Gold Nanostructures with Hidden Tags (BRIGHTs) for High-Resolution Bioimaging, Advanced Materials, 25 (2013) 1022-1027.
[101] C. Hu, J. Shen, J. Yan, J. Zhong, W. Qin, R. Liu, A. Aldalbahi, X. Zuo, S. Song, C. Fan, D. He, Highly narrow nanogap-containing Au@Au core-shell SERS nanoparticles: size-dependent Raman enhancement and applications in cancer cell imaging, Nanoscale, 8 (2016) 2090-2096.
[102] P. Lang, K. Yeow, A. Nichols, A. Scheer, Cellular imaging in drug discovery, Nat Rev Drug Discov, 5 (2006) 343-356.
[103] J.A. Ludwig, J.N. Weinstein, Biomarkers in Cancer Staging, Prognosis and Treatment Selection, Nature Reviews Cancer, 5 (2005) 845-856.

[104] S. Lee, H. Chon, J. Lee, J. Ko, B.H. Chung, D.W. Lim, J. Choo, Rapid and sensitive phenotypic marker detection on breast cancer cells using surface-enhanced Raman scattering (SERS) imaging, Biosensors and Bioelectronics, 51 (2014) 238-243.
[105] U.S. Dinish, G. Balasundaram, Y.-T. Chang, M. Olivo, Actively Targeted In Vivo Multiplex Detection of Intrinsic Cancer Biomarkers Using Biocompatible SERS Nanotags, Scientific Reports, 4 (2014).
[106] Z.A. Nima, M. Mahmood, Y. Xu, T. Mustafa, F. Watanabe, D.A. Nedosekin, M.A. Juratli, T. Fahmi, E.I. Galanzha, J.P. Nolan, A.G. Basnakian, V.P. Zharov, A.S. Biris, Circulating tumor cell identification by functionalized silver-gold nanorods with multicolor, super-enhanced SERS and photothermal resonances, Scientific Reports, 4 (2014).
[107] G. Bodelón, V. Montes-García, C. Fernández-López, I. Pastoriza-Santos, J. Pérez-Juste, L.M. Liz-Marzán, Au@pNIPAM SERRS Tags for Multiplex Immunophenotyping Cellular Receptors and Imaging Tumor Cells, Small, 11 (2015) 4149-4157.
[108] J. Wessel, Surface-enhanced optical microscopy, Journal of the Optical Society of America B, 2 (1985) 1538.
[109] N. Hayazawa, Y. Inouye, Z. Sekkat, S. Kawata, Metallized tip amplification of near-field Raman scattering, Optics Communications, 183 (2000) 333-336.
[110] M.S. Anderson, Locally enhanced Raman spectroscopy with an atomic force microscope, Applied Physics Letters, 76 (2000) 3130.
[111] R.M. Stöckle, Y.D. Suh, V. Deckert, R. Zenobi, Nanoscale chemical analysis by tip-enhanced Raman spectroscopy, Chemical Physics Letters, 318 (2000) 131-136.
[112] V. Deckert, T. Deckert-Gaudig, M. Diegel, I. Götz, L. Langelüddecke, H. Schneidewind, G. Sharma, P. Singh, P. Singh, S. Trautmann, M. Zeisberger, Z. Zhang, Spatial resolution in Raman spectroscopy, Faraday Discuss., 177 (2015) 9-20.
[113] R. Zhang, Y. Zhang, Z.C. Dong, S. Jiang, C. Zhang, L.G. Chen, L. Zhang, Y. Liao, J. Aizpurua, Y. Luo, J.L. Yang, J.G. Hou, Chemical mapping of a single molecule by plasmon-enhanced Raman scattering, Nature, 498 (2013) 82-86.
[114] Z. Yang, J. Aizpurua, H. Xu, Electromagnetic field enhancement in TERS configurations, Journal of Raman Spectroscopy, 40 (2009) 1343-1348.
[115] D. Mehtani, N. Lee, R.D. Hartschuh, A. Kisliuk, M.D. Foster, A.P. Sokolov, J.F. Maguire, Nano-Raman spectroscopy with side-illumination optics, Journal of Raman Spectroscopy, 36 (2005) 1068-1075.
[116] R. Ossikovski, Q. Nguyen, G. Picardi, Simple model for the polarization effects in tip-enhanced Raman spectroscopy, Physical Review B, 75 (2007).
[117] J.M. Marr, Z.D. Schultz, Imaging Electric Fields in SERS and TERS Using the Vibrational Stark Effect, The Journal of Physical Chemistry Letters, 4 (2013) 3268-3272.
[118] M.D. Sonntag, J.M. Klingsporn, L.K. Garibay, J.M. Roberts, J.A. Dieringer, T. Seideman, K.A. Scheidt, L. Jensen, G.C. Schatz, R.P. Van Duyne, Single-Molecule Tip-Enhanced Raman Spectroscopy, The Journal of Physical Chemistry C, 116 (2012) 478-483.
[119] L. Langelüddecke, P. Singh, V. Deckert, Exploring the Nanoscale: Fifteen Years of Tip-Enhanced Raman Spectroscopy, Applied Spectroscopy, 69 (2015) 1357-1371.
[120] L. Opilik, T. Bauer, T. Schmid, J. Stadler, R. Zenobi, Nanoscale chemical imaging of segregated lipid domains using tip-enhanced Raman spectroscopy, Physical Chemistry Chemical Physics, 13 (2011) 9978.
[121] A. Nakata, T. Nomoto, T. Toyota, M. Fujinami, Tip-enhanced Raman spectroscopy of lipid bilayers in water with an alumina- and silver-coated tungsten tip, Anal Sci, 29 (2013) 865-869.

[122] M. Richter, M. Hedegaard, T. Deckert-Gaudig, P. Lampen, V. Deckert, Laterally Resolved and Direct Spectroscopic Evidence of Nanometer-Sized Lipid and Protein Domains on a Single Cell, Small, 7 (2011) 209-214.
[123] R. Böhme, M. Richter, D. Cialla, P. Rösch, V. Deckert, J. Popp, Towards a specific characterisation of components on a cell surface-combined TERS-investigations of lipids and human cells, Journal of Raman Spectroscopy, 40 (2009) 1452-1457.
[124] R. Böhme, D. Cialla, M. Richter, P. Rösch, J. Popp, V. Deckert, Biochemical imaging below the diffraction limit - probing cellular membrane related structures by tip-enhanced Raman spectroscopy (TERS), Journal of Biophotonics, 3 (2010) 455-461.
[125] K.D. Alexander, Z.D. Schultz, Tip-Enhanced Raman Detection of Antibody Conjugated Nanoparticles on Cellular Membranes, Analytical Chemistry, 84 (2012) 7408-7414.
[126] H. Wang, Z.D. Schultz, TERS Detection of αVβ3Integrins in Intact Cell Membranes, Chemphyschem, 15 (2014) 3944-3949.
[127] L. Xiao, H. Wang, Z.D. Schultz, Selective Detection of RGD-Integrin Binding in Cancer Cells Using Tip Enhanced Raman Scattering Microscopy, Anal Chem, 88 (2016) 6547-6553.
[128] U. Neugebauer, P. Rösch, M. Schmitt, J. Popp, C. Julien, A. Rasmussen, C. Budich, V. Deckert, On the Way to Nanometer-Sized Information of the Bacterial Surface by Tip-Enhanced Raman Spectroscopy, Chemphyschem, 7 (2006) 1428-1430.
[129] U. Neugebauer, U. Schmid, K. Baumann, W. Ziebuhr, S. Kozitskaya, V. Deckert, M. Schmitt, J. Popp, Towards a Detailed Understanding of Bacterial Metabolism—Spectroscopic Characterization ofStaphylococcus Epidermidis, Chemphyschem, 8 (2007) 124-137.
[130] D. Cialla, T. Deckert-Gaudig, C. Budich, M. Laue, R. Möller, D. Naumann, V. Deckert, J. Popp, Raman to the limit: tip-enhanced Raman spectroscopic investigations of a single tobacco mosaic virus, Journal of Raman Spectroscopy, 40 (2009) 240-243.
[131] P. Hermann, A. Hermelink, V. Lausch, G. Holland, L. Möller, N. Bannert, D. Naumann, Evaluation of tip-enhanced Raman spectroscopy for characterizing different virus strains, The Analyst, 136 (2011) 1148.
[132] K. Olschewski, E. Kämmer, S. Stöckel, T. Bocklitz, T. Deckert-Gaudig, R. Zell, D. Cialla-May, K. Weber, V. Deckert, J. Popp, A manual and an automatic TERS based virus discrimination, Nanoscale, 7 (2015) 4545-4552.
[133] J.M. Klingsporn, M.D. Sonntag, T. Seideman, R.P. Van Duyne, Tip-Enhanced Raman Spectroscopy with Picosecond Pulses, The Journal of Physical Chemistry Letters, 5 (2014) 106-110.
[134] J.A. Prescher, C.R. Bertozzi, Chemistry in living systems, Nature Chemical Biology, 1 (2005) 13-21.
[135] V.V. Rostovtsev, L.G. Green, V.V. Fokin, K.B. Sharpless, A Stepwise Huisgen Cycloaddition Process: Copper(I)-Catalyzed Regioselective "Ligation" of Azides and Terminal Alkynes, Angewandte Chemie International Edition, 41 (2002) 2596-2599.
[136] C.W. Tornøe, C. Christensen, M. Meldal, Peptidotriazoles on Solid Phase: [1,2,3]-Triazoles by Regiospecific Copper(I)-Catalyzed 1,3-Dipolar Cycloadditions of Terminal Alkynes to Azides, The Journal of Organic Chemistry, 67 (2002) 3057-3064.
[137] J.M. Baskin, J.A. Prescher, S.T. Laughlin, N.J. Agard, P.V. Chang, I.A. Miller, A. Lo, J.A. Codelli, C.R. Bertozzi, Copper-free click chemistry for dynamic in vivo imaging, Proceedings of the National Academy of Sciences, 104 (2007) 16793-16797.

[138] H. Yamakoshi, K. Dodo, M. Okada, J. Ando, A. Palonpon, K. Fujita, S. Kawata, M. Sodeoka, Imaging of EdU, an Alkyne-Tagged Cell Proliferation Probe, by Raman Microscopy, Journal of the American Chemical Society, 133 (2011) 6102-6105.
[139] H. Yamakoshi, K. Dodo, A. Palonpon, J. Ando, K. Fujita, S. Kawata, M. Sodeoka, Alkyne-Tag Raman Imaging for Visualization of Mobile Small Molecules in Live Cells, Journal of the American Chemical Society, 134 (2012) 20681-20689.
[140] L. Wei, F. Hu, Y. Shen, Z. Chen, Y. Yu, C.-C. Lin, M.C. Wang, W. Min, Live-cell imaging of alkyne-tagged small biomolecules by stimulated Raman scattering, Nature Methods, 11 (2014) 410-412.
[141] A. Alfonso-García, S.G. Pfisterer, H. Riezman, E. Ikonen, E.O. Potma, D38-cholesterol as a Raman active probe for imaging intracellular cholesterol storage, Journal of Biomedical Optics, 21 (2015) 061003.
[142] Z. Chen, D.W. Paley, L. Wei, A.L. Weisman, R.A. Friesner, C. Nuckolls, W. Min, Multicolor Live-Cell Chemical Imaging by Isotopically Edited Alkyne Vibrational Palette, Journal of the American Chemical Society, 136 (2014) 8027-8033.
[143] Y. Chen, J.-Q. Ren, X.-G. Zhang, D.-Y. Wu, A.-G. Shen, J.-M. Hu, Alkyne-Modulated Surface-Enhanced Raman Scattering-Palette for Optical Interference-Free and Multiplex Cellular Imaging, Analytical Chemistry, 88 (2016) 6115-6119.
[144] Z. Liu, S. Tabakman, K. Welsher, H. Dai, Carbon Nanotubes in Biology and Medicine: In vitro and in vivo Detection, Imaging and Drug Delivery, Nano Res, 2 (2009) 85-120.
[145] Z. Liu, S.M. Tabakman, Z. Chen, H. Dai, Preparation of carbon nanotube bioconjugates for biomedical applications, Nature Protocols, 4 (2009) 1372-1381.
[146] Z. Liu, X. Li, S.M. Tabakman, K. Jiang, S. Fan, H. Dai, Multiplexed Multicolor Raman Imaging of Live Cells with Isotopically Modified Single Walled Carbon Nanotubes, Journal of the American Chemical Society, 130 (2008) 13540-13541.
[147] Z. Liu, S. Tabakman, S. Sherlock, X. Li, Z. Chen, K. Jiang, S. Fan, H. Dai, Multiplexed five-color molecular imaging of cancer cells and tumor tissues with carbon nanotube Raman tags in the near-infrared, Nano Research, 3 (2010) 222-233.

Figures and Tables

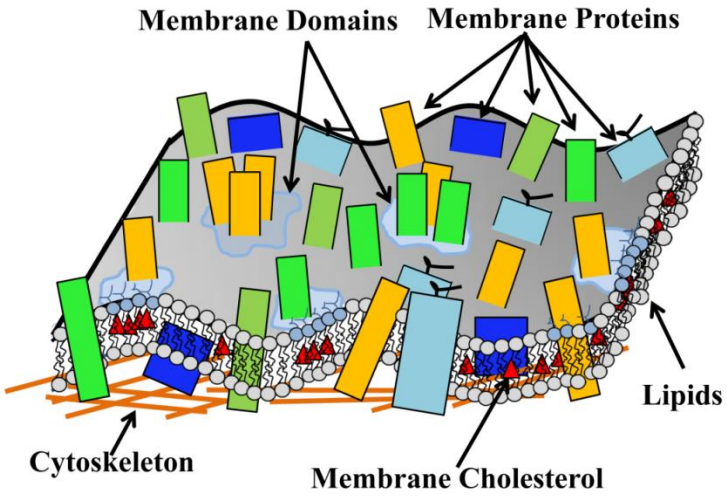

Figure 1. Schematic depicting the organization of cell membrane and associated components. As with most figures of membrane structure, for simplicity this schematic does not represent the true membrane crowding.

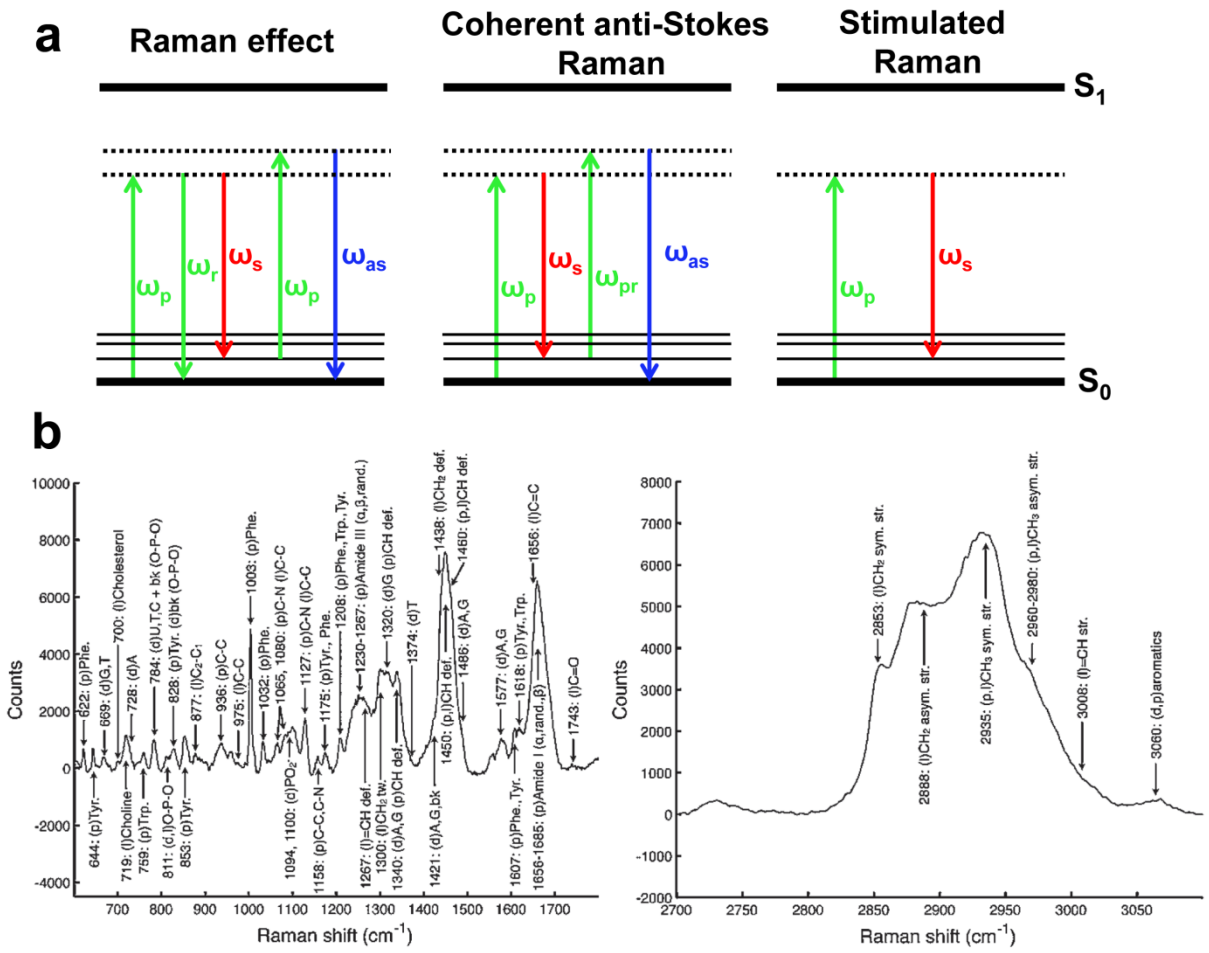

Figure 2. (a) Jablonski diagrams depicting spontaneous and nonlinear Raman processes. Symbols—ω_p: pump frequency, ω_r: Rayleigh frequency, ω_s: Stokes frequency, ω_{pr}: probe frequency, ω_{as}: anti-Stokes frequency. (b) Raman spectra of a single human tumor cell. Peaks are shown in the fingerprint region (500 cm^{-1} to 1800 cm^{-1}) and C-H stretching region (2700 cm^{-1} to 3100 cm^{-1}). Abbreviations—p: protein, l: lipid, d: DNA/RNA, A: adenine, T: thymine, G: guanine, C: cytosine, U: uracil, Phe: phenylalanine, Tyr: tyrosine, Trp: tryptophan, bk: backbone, def: deformation, tw: twist, sym: symmetric, asym: asymmetric, str: stretch (© Institute of Physics and Engineering in Medicine. Reproduced from reference [12] with permission of IOP Publishing. All rights reserved. DOI:10.1088/0031-9155/56/1/002).

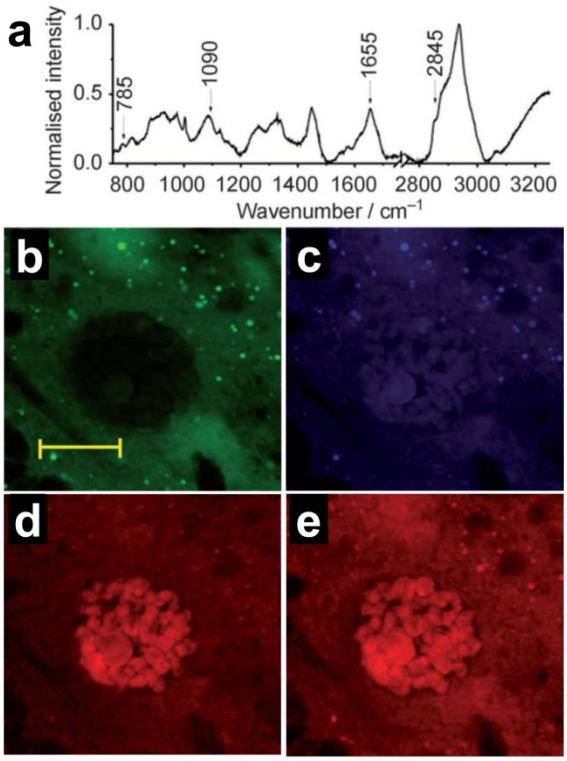

Figure 3. (a) Spontaneous Raman spectrum of a Drosophila cell. SRS image of a single cell obtained for lipids at (b) 2845 cm^{-1}, protein at (c) 1655 $cm^{-1,}$, nucleic acids at (d) 785 cm^{-1} and (e) 1090 cm^{-1}. The scale bar is 20 μm. (Reproduced from reference [52] with permission from John Wiley and Sons).

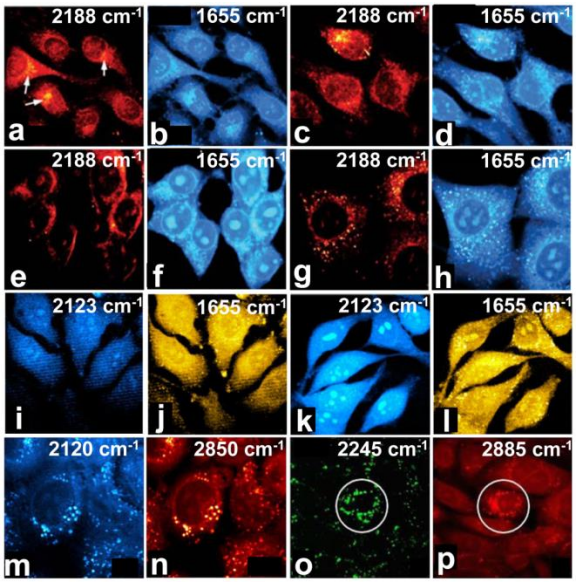

Figure 4. SRS images. (a-h) Distribution of deuterated choline-containing metabolites (C-D peak at 2188 cm^{-1}) and as a control protein distribution (amide I peak at 1655 cm^{-1}) imaged in (a-b) HeLa, (c-d) U2OS, (e-f) HEK293T and (g-h) NIH3T3 cells. (Reproduced from reference [59] with permission from Royal Society of Chemistry. DOI:10.1039/C3AN02281A). (i) and (k) Time-dependent chemical imaging of newly synthesized proteins labeled with deuterated amino acids in HeLa cells at 5 h and 20 h, respectively, (j) and (l) control total protein distribution (amide I peak at 1655 cm^{-1}) imaged at 5 h and 20 h, respectively [58]. (m) Distribution of newly synthesized lipids from deuterated glucose (C-D peak at 2120 cm^{-1}) and (n) control, total lipid distribution (C-H peak at 2850 cm^{-1}) imaged in pancreatic cancer cells [57]. (o) Cell Membrane distribution of phenyl-diyne labeled cholesterol (C-D peak at 2245 cm^{-1}), and (p) lipid signal (C-H peak at 2885 cm^{-1}) imaged in a live CHO cell [60].

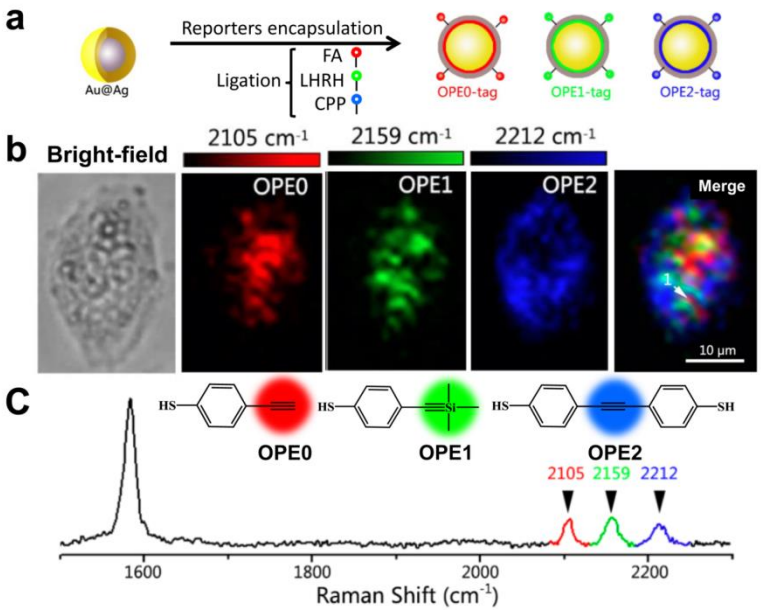

Figure 5. Multicolor SERS imaging in live HeLa cells. (a) Schematic representation of three alkyne-tagged SERS reporters with surface-ligation for targeting folic acid (FA) receptor (OPE0), luteinizing hormone-releasing hormone (LHRH) receptor (OPE1), and polypeptide chain containing multiple arginine (CPP) for cytoplasmic localization (OPE2). (b) Bright-field and SERS images of each of the three SERS reporters as well as an overlaid image of all three images. (c) The Raman spectrum from the location shown with a white arrow in the overlay image and corresponding chemical structure of each Raman reporter. (Adapted with permission from (Analytical Chemistry, 2016, 88, 6115-6119). Copyright (2016) American Chemical Society.)

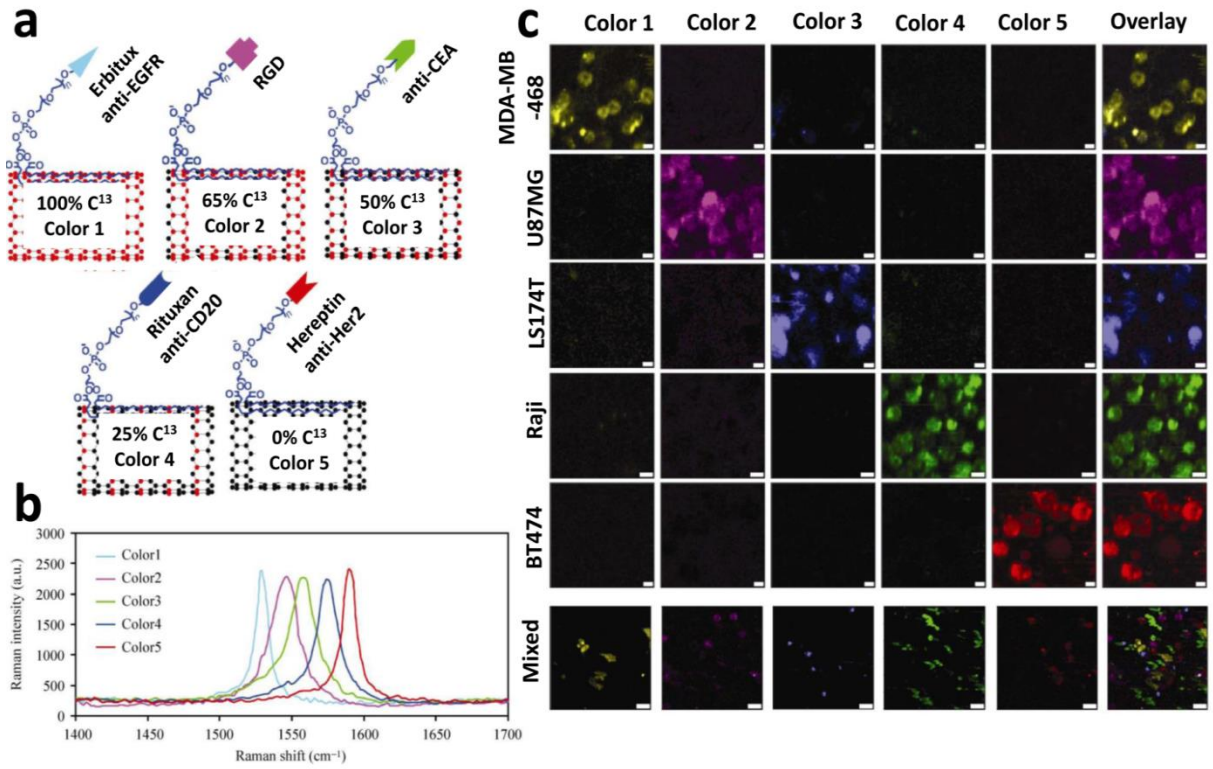

Figure 6. Multi-color Raman imaging with SWNTs. (a) Isotopically modified SWNTs with a specific antibody or peptide to target a surface biomarker on a cancer cell membrane. (b) Peak location of G-band for each SWNTs shown in (a). (c) Five color Raman imaging of five cancer cell-types containing different biomarkers (MDA-MB-468, U87MG, LS174T, Raji, and BT474) using the indicated SWNT. As a control, in the mixed samples, all five cancer cells are mixed and incubated with the five-color SWNT mixture. Abbreviations—EGFR: epidermal growth factor receptor; RGD: peptide targeting integrins; CEA: carcinoembryonic antigen; CD20: B-lymphocyte antigen; Her2: receptor tyrosine-protein kinase erB-2. The scale bars are 10 μm for the top five rows and 40 μm in the bottom row [147].